AIAA SciTech Forum
12-16 January 2026, Orlando, FL
AIAA SCITECH 2026 Forum

10.2514/6.2026-1549

Preliminary Analysis of the Wake Region in Hypersonic Aerobreakup

J. D. Langhorn*, A. R. Dworzanczyk†, A. J. Marino‡, and N. J. Parziale§
Stevens Institute of Technology, Hoboken, New Jersey 07030, USA

F. J. Ayoub¶, M. Viqueira-Moreira‖, and C. Brehm**
University of Maryland, College Park, MD 20742, USA

M. A. Libeau††
Naval Surface Warfare Center Dahlgren Division, Dahlgren, Virginia, 22448, USA

The aerobreakup of liquid drops along the stagnation streamline of flat-faced, high-speed projectiles ($3.03 \leq M_p \leq 5.12$) was studied in Dworzanczyk et al. [1]. In that work, the authors provide a database of computational and experimental results. The length and structure of the drop wake region is analyzed in more detail in this paper. Computations were performed with and without viscosity and surface tension; these results show that these parameters don't change the wake structure significantly. This indicates that the Weber and Reynolds numbers may not be the most meaningful nondimensional numbers in this application. However, the structure of the wake was observed to be strongly dependent on the local Mach number of the flow, in the drop frame of reference. The computational and experimental results show that Mach number has a pronounced effect on two fundamental aspects of the flow: the flow expansion angle around the droplet geometry and the underlying stability characteristics of the shear layer. That is, there is a stabilizing effect of increasing Mach number where the local Mach number is in the 1-2 range.

I. Nomenclature

a_g	=	sound speed of the gas
γ	=	heat capacity ratio
d	=	instantaneous drop diameter
d_0, D	=	initial drop diameter
L	=	wake length
M	=	Mach number
M_{2LF}	=	Mach number of the gas immediately behind the projectile bow shock in the drop reference frame
M_p	=	Mach number of the projectile
μ_g	=	dynamic viscosity of the gas
P_2	=	pressure of the gas immediately behind the projectile bow shock
ρ_2	=	density of the gas immediately behind the projectile bow shock
ρ_d	=	drop density
ρ_g	=	gas density
Re_{A2}	=	Reynolds number of the gas immediately behind the projectile bow shock
Re_D	=	Reynolds number of the liquid flow within the drop

*Graduate Student, Mechanical Engineering, 1 Castle Point on Hudson, Hoboken, New Jersey 07030.
†Graduate Student, Mechanical Engineering, 1 Castle Point on Hudson, Hoboken, New Jersey 07030.
‡Graduate Student, Mechanical Engineering, 1 Castle Point on Hudson, Hoboken, New Jersey 07030.
§George Meade Bond Professor, Mechanical Engineering, 1 Castle Point on Hudson, Hoboken, New Jersey, 07030, AIAA Associate Fellow.
¶Graduate Student, Aerospace Engineering Department, University of Maryland, College Park, MD 20742, USA
‖Faculty Assistant, Aerospace Engineering Department, University of Maryland, College Park, MD 20742, USA
**Associate Professor, Aerospace Engineering Department, University of Maryland, College Park, MD 20742, USA
††Hypersonic Technology Chief Scientist, Integrated Engagement Systems Department, Dahlgren, Virginia, 22448, USA.

σ = Surface Tension
T_2 = temperature of the gas immediately behind the projectile bow shock
τ = non-dimensional time
t = time
t_{c2} = characteristic breakup time
U_A = gas velocity, relative to the drop velocity
We_{A2} = Weber number using properties of the gas immediately behind the projectile bow shock

II. Introduction

Aerobreakup, or the process by which a liquid mass is aerodynamically deformed and degraded by a high-speed gaseous flow, is a necessary consideration for a variety of modern engineering problems. This includes the modeling of liquid molt in metal powder manufacturing [2–4], liquid fuel in high-speed combustion/detonation [5–7], and liquid precipitation in high-speed-vehicle/weather encounters [1, 8–14]. This effort specifically, is performed in the context of high-speed weather encounters.

Studies of aerobreakup are often classified via the Weber number, expressed as $We_A = (\rho_g U_A^2 d_0)/\sigma$. Here, the Weber number nondimensionalizes the magnitude of the expected destructive aerodynamic forces on the drop by that of the stabilizing surface tension forces at the gas-liquid interface. As the Weber number increases, the effects of surface tension become dwarfed by the increasingly violent aerodynamic effects. Pilch and Erdman [15] gives a thorough review of the expected behavior of a liquid mass experiencing low Weber aerobrerakup ($We < 350$). At higher Weber numbers, however, the literature begins to reveal discrepancies in the predicted breakup modes and mechanisms. This led some researchers to posit that in cases of extremely violent aerobreakup, the Weber number alone is insufficient in determining the breakup behavior/mechanisms [1]. As a result, this study will consider effects of gaseous compressibility (expressed via the Mach number, $M_A = U_A/a_g$), gaseous viscosity/turbulence (expressed via the Reynolds number, $Re_A = \rho_g U_A d_0/\mu_g$), and the acceleration of the liquid mass (expressed via the nondimensional time, $\tau = t/t_{C2} = tU_A\sqrt{\rho_g}/d_0\sqrt{\rho_d}$).

Dworzanczyk et al. [1] studied the aerobreakup problem via experiments and computations of individual, isolated water drops on a series of flat-faced, supersonic projectiles ($3.03 \leq M_p \leq 5.12$). This enabled the authors to record not only the deformation and displacement of the drop, but also the evolution of the windward multiphase instabilities and the shock structure development about the drop with good spatial and temporal resolution. The lack of experimental obscurities allowed for near one-to-one comparisons with the simulations, providing further validation to the code. For the purpose of predicting the aerobreakup of individual drops, Dworzanczyk et al. [1] provides a useful analysis. In practical application, however, it is likely that the subject of the aerobreakup problem will not be a single drop, but rather a cloud liquid drops. In this case, the downstream drops may not experience the same freestream flow field that processed the upstream drops. Hence, to capture the effects of aerobreakup as it pertains to a collection of liquid drops, the modification of the downstream flow by upstream drops must be studied.

In this paper, we utilize the dataset provided by Dworzanczyk et al. [1] to perform a preliminary analysis of the wake region of liquid drops during aerobreakup. The wake dynamics were not examined in detail in the original work; however, the observed wake length exhibited a strong dependence on Mach number, a trend captured consistently in both the simulations and the experiments. The present paper offers a preliminary investigation aimed at elucidating the flow physics underlying this highly complex multiphase wake. The paper provides a brief overview of the experimental setup and the numerical modeling approach, followed by a comparison of the experimental flow visualizations with the simulation results. It concludes with a discussion of potential mechanisms responsible for the observed short- and long-wake behavior.

III. Experimental and Computational Design

Dworzanczyk et al. [1] recorded high-speed shadowgraph of the aerobreakup and impingement of liquid drops ($0.51\text{ mm} \leq d_0 \leq 2.30\text{ mm}$) near and on the surface of a series of flat-faced, supersonic projectiles ($3.03 \leq M_P \leq 5.12$). This was made possible through the use of a large-caliber electromagnetic launcher (EML), located in the Potomac River Test Range at the Naval Surface Warfare Center Dahlgren Division [16]. Some of the resulting shadowgraphs of "Drop 3" are shown in Fig. 1 to provide context for further analysis.

The EML experiments were performed outdoors in a standard sea-level environment. Dworzanczyk et al. [1] employ a one-dimensional, reacting gasdynamics model to estimate the properties of the fluid within the shock standoff region

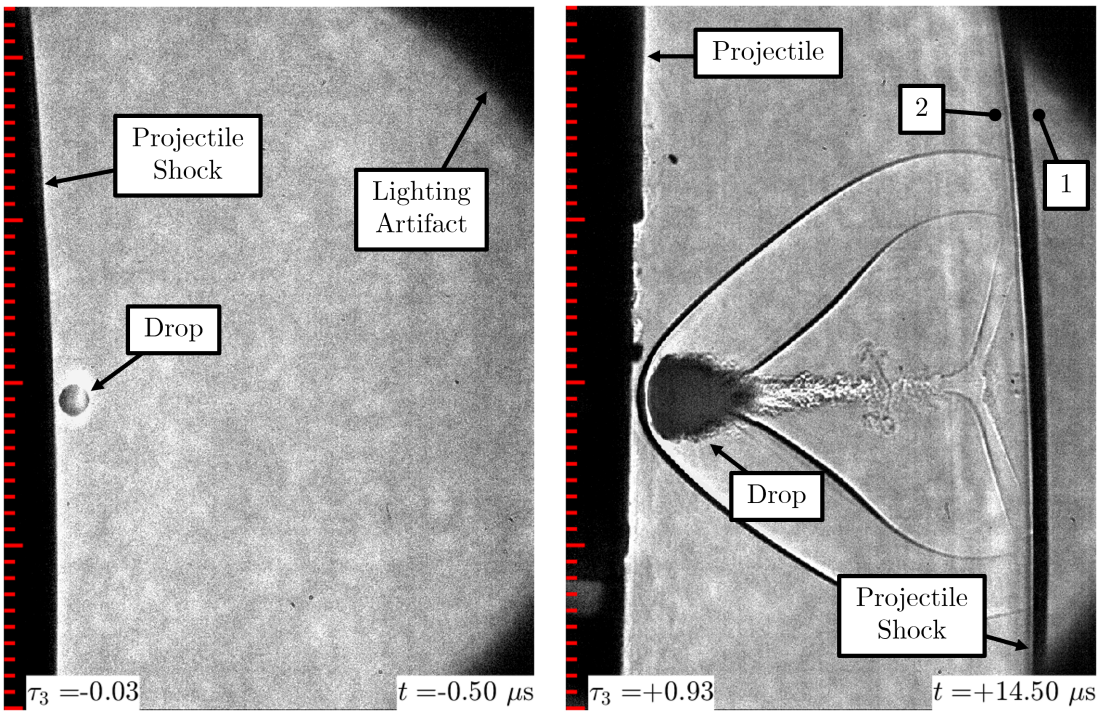

(a) **(b)**

Fig. 1 Shadowgraphy of a liquid water drop before (1a) and after (1b) significant aerobreakup induced by the high-speed gas proceeding a rightward-moving, supersonic projectile [1]. In both images, the red tick marks denote millimeter increments, and both the dimensional and nondimensional time since the passage of the projectile bow shock over the liquid drop are given in the bottom right and bottom left corners, respectively. Notable features within the shadowgraphy are called out. The numbers 1 and 2 correspond to the points immediately before and after the projectile bow shock.

of the projectile. In this study, we will consider only two drops—a high speed case (Drop 3) and a low speed case (Drop 6B). The relevant dimensional and nondimensional parameters are summarized in Tab. 1. To remain consistent with the nomenclature of the original authors, the properties of the gas immediately behind the projectile bow shock are assigned the subscript 2. Dimensional and nondimensional velocities that are estimated in the "laboratory reference frame," (or measured relative to the velocity of the drop) are appended with "LF" in the subscript.

Numerical models[10, 11, 17, 18] were also used in conjunction with the experimental setup to further the depth of data analysis. A viscous five-equation model was adopted from Allaire et al. [19]. This equation uses a combination of mass conservation, momentum, energy, and non-conservative volume fraction equations to properly solve for the multiphase nature of droplet breakup. This model offered good comparisons with high Mach number experimental instability data, further reinforcing its viability within this research.

The equations of the previously mentioned model were solved using a fifth-order weighted compact nonlinear scheme developed by Wong et al. [20]. This solver utilizes a higher-order flux and variable reconstruction, positively

Drop	M_P	d_0	U_{2LF}	T_2	P_2	ρ_2	M_{2LF}	We_{A2}	Re_{A2}
(-)	(-)	(mm)	(m/s)	(K)	(kPa)	(kg/m^3)	(-)	(-)	(-)
3	5.12	1.87	1461	1639	3138	6.62	1.86	3.69e5	3.07e5
6B	3.03	1.27	790	793	1071	4.68	1.42	5.17e4	1.28e5

Table 1 Relevant aerobreakup conditions reported by Dworzanczyk et al. [1]

preserving the limiting procedure, and a first-order Harten-Lax-van Leer contact Riemann solver. The viscous terms are then discretized by using a regular centered second-order finite difference discretization. A Runge-Kutta method is also used for time integration.

An immersed boundary method [21–23] is utilized to simulate the experiment. A perfect gas flow field over the projectile is computed, which allows a shock to form. A drop is then placed in front of it, and the resulting aerodynamic characteristics are recorded. Adaptive mesh refinement is used for computational efficiency. 12 refinement levels and 150 grid points per diameter were used for the simulation's resolution.

IV. Wake Dynamics

In Fig. 2, we present drop shadowgraphs from the experiment and computations for Drops 3 and 6B. A numerical shadowgraph is obtained by painting the three-dimensional 0.1% water volume fraction contour black to mimic what the camera sees. An inverse correlation of wake length to Mach number is visually apparent in Fig. 2 and is captured in both the experiments and the simulations. The close agreement between the experiments and simulations provides some confidence that the simulations can capture the dominant flow physics driving the aerobreakup mechanisms. Hence, as the differences in the wakes between Drop 3 and Drop 6B are consistent between both the simulations and the experiments, we can use the simulation results to gain further insights into the dominant flow physics.

An additional qualitative difference between Drop 3 and Drop 6B is the opacity of the wake. For the higher-Mach-number Drop 3 case, the wake appears significantly less opaque in the experimental shadowgraphs, whereas the lower-Mach-number Drop 6B wake remains comparatively opaque. Since the numerical shadowgraphs are generated by thresholding the liquid volume fraction, variations in optical transparency cannot be represented. The reduced opacity observed for Drop 3 may therefore indicate possible phase transition, the presence of evaporation, or a transition toward supercritical fluid states in the wake, which are not accounted for in the present model. While this interpretation is not conclusive, it points to thermodynamic effects that may become relevant at higher Mach numbers.

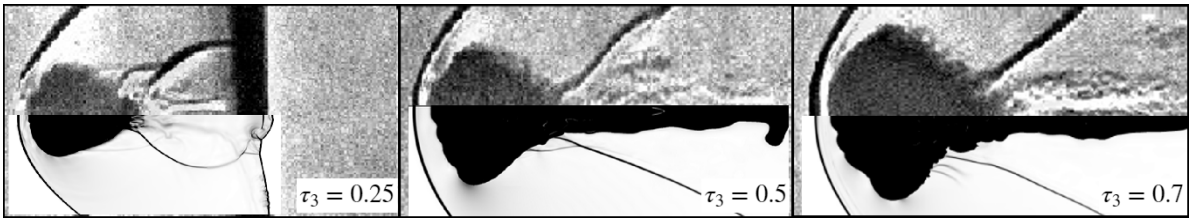

(a) Drop 3 ($M_{2LF} = 1.86$)

(b) Drop 6B (M_{2LF}1.42)

Fig. 2 A comparison of experimental (top) and computational (bottom) shadowgraphy for Drop 3 (a) and Drop 6B (b) over a range of nondimensional times. The projectile is moving from left to right, and the nondimensional time for each comparison is given in the bottom right corner. Computational shadowgraphs are made by visualizing a 0.1% liquid volume fraction.

The wake length versus time for Drop 3 and Drop 6B is shown in Fig. 3a for experiments and computations, with nominal agreement. The wake length is normalized by the instantaneous drop radius ($L(2/d)$). When plotted this way, the ordinate will be equal to the cotangent of the flow angle. Hence, when the ordinate remains at a constant value, the flow angle must also be constant, and geometric self-similarity can be inferred. The time scale is normalized by the kinematic timescale, U_{2LF}/d_0. This implies that the wake constituency is nearly following the streamlines of the flow. Drop 6b grows linearly until mass shedding at $tU_{2LF}/d_0 = 10$. The Drop 3 wake length appears to be self-similar, as $L(2/d) \approx$ constant. The self similar versus linear growth between the low and high Mach number cases indicates a

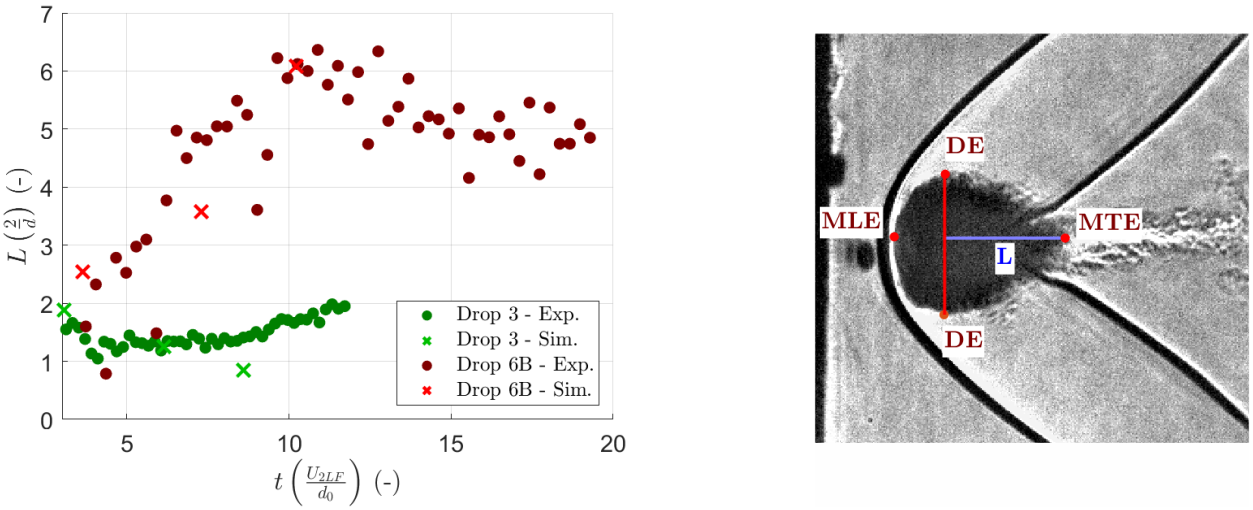

(a) **(b)**

Fig. 3 The observed wake length, normalized by the instantaneous drop radius, plotted over nondimensional time (a). An experimental shadowgraph of Drop 3 undergoing aerobreakup (b). The mist leading edge (MLE), drop equator (DE), and mist trailing edge (MTE) are called out. A vertical red line splits the horizontal position of the two drop equator points. The horizontal distance from the drop equator to the MTE will be defined as the wake length (L).

strong parametric effect worthy of further inspection.

Fig. 4 shows three water volume fraction contour lines with volume fractions of 0.1%, 1%, and 10% in a cut-plane through the center of the drop for the Drops 3 and 6B. It appears that the wake for the lower Mach number case breaks up more quickly which subsequently significantly alters the downstream wake flow features. We can gain some insights into what physical mechanisms are dominant when considering the limitations in the flow physics that can be captured with the current simulation approach. The current simulation approach does not account for surface tension effects, thus, surface tension effects can be disregarded, which also means the Weber number will not be a relevant flow parameter to explain the differences in the wake dynamics. Furthermore, it was observed that when comparing viscous versus inviscid simulations the wake dynamics are not significantly altered. Moreover, the grid resolution in the current simulation is not sufficient to properly capture the thin boundary-layer flow around the drop, a difficult task with a Cartesian grid-based method. Hence, it can be assumed that viscous effects are likely not to dominate the behavior observed in the simulations/experiments. However, it should be noted that even though a higher-order fifth-order accurate scheme has been used, numerical dissipation through the discretization of the convective terms will affect the small-scale flow features effectively acting as an implicit filter.

The only remaining parameter is the Mach number. Therefore, although the differences in Mach number are only approximately 25%, it appears that the Mach number could be an important parameter affecting the dynamics of the wake flow. The obvious question to be answered is: How could such a small difference in Mach number cause such a strong effect on the wake dynamics? To understand this, the full Mach number distribution around the drop needs to be considered, in particular, the Mach number distribution in the wake region. The inset of Mach number at $\tau = 0.25$ in Fig. 4, a time instant before the wake has started to break up, clearly shows that the Mach number in the wake of Drop 6B is substantially lower than for Drop 3. Established stability analysis results for wake flows seem to be able to give a reasonable explanation about the dynamics observed in the wake of the drops. In several stability analyses of wake and shear-layer flows over a wide range of Mach numbers, it has been shown that the Mach number has a stabilizing effect on wake instabilities [24–26]. These studies also show a rapid reduction of the growth rates in the Mach number range 1-2 which falls within the Mach number ranges relevant for Drops 6B and 3, as $M_{2LF} = 1.42, 1.86$. Part of the explanation for the differences in wake dynamics is that the wake structures observed for the low and high Mach numbers are affected by the stabilizing influence of increasing Mach number (or compressibility effects) on the shear-layer instabilities that form in the drop's wake. As the Mach number increases, these instabilities become progressively more stable, leading to an inherent delay in the onset of wake breakup.

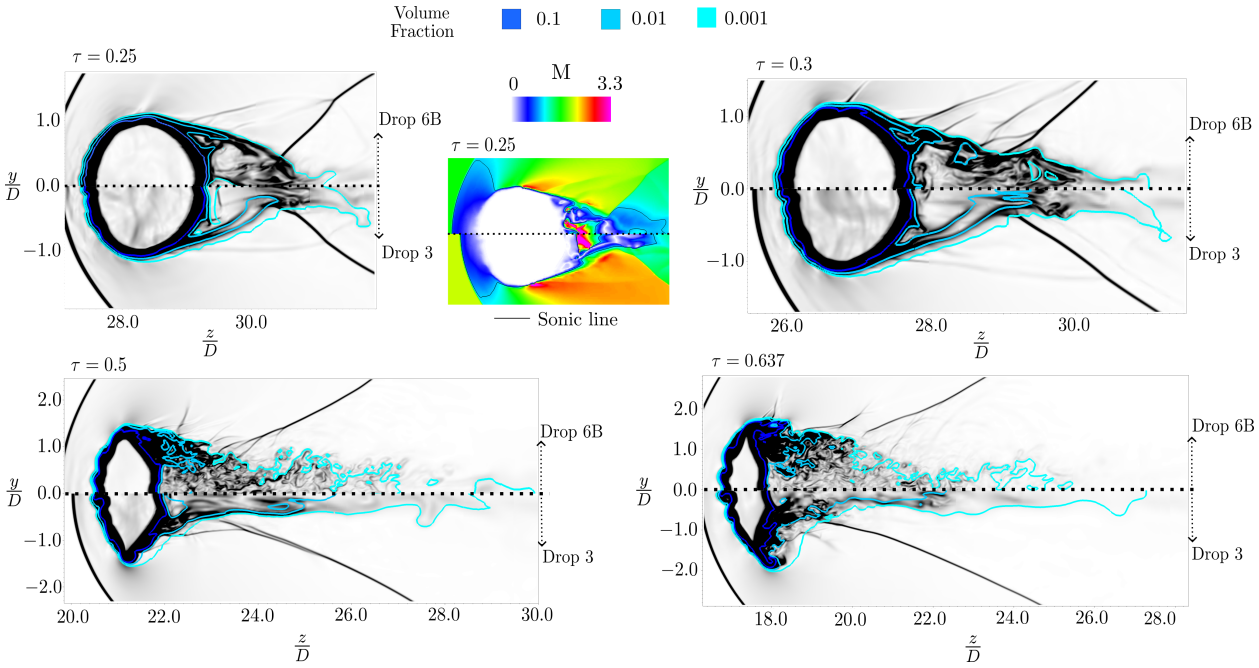

Fig. 4 Comparison of Drop 3 and Drop 6B wake development through visualization of water volume fractions.

In addition to the Mach-number–dependent stability characteristics of the shear layer, the flow expansion around the droplet is also significantly altered. As discussed in [27–29] the expansion angle depends strongly on both Mach number and base pressure. To assess this effect, we conducted numerical simulations using the GPU-accelerated CHAMPS+ CFD solver [30] considering a perfect-gas flow with $\gamma = 1.4$ and $Re_D \approx 50{,}000$ (lower than in the droplet experiments and simulations) around a smooth sphere at various Mach numbers. Although the Reynolds number is too low to produce rapid shear-layer breakup (even in the lower Mach-number case), the results clearly show that the expansion angle is influenced by Mach number: at higher Mach numbers, the flow exhibits a noticeably larger expansion angle. Fig. 5 presents Mach-number contours and surface-pressure distributions for the cases with $M = 1.25$, 1.5, 1.75, and 2.0. The flow expansion around the crest of the sphere is clearly evident in the Mach-number fields. While these perfect-gas, smooth-sphere simulations cannot capture the full complexity of a multiphase gas–liquid wake, such as variations in specific heat ratio (even if modest), changes in droplet shape during breakup, or the presence of a non-zero wall-velocity boundary layer, the dominant Mach-number effect on flow expansion is expected to persist.

V. Conclusion

A preliminary analysis of the wake region behind a liquid drop during high-speed aerobreakup is performed. The shadowgraphy of Dworzanczyk et al. [1] is analyzed and compared to simulations with good qualitative and quantitative agreement. The differences in the wake lengths and shear-layer instabilities of a high-Mach number case (Drop 3) and a low-Mach number case (Drop 6B) are analyzed. Despite changes in the drop diameter, geometric self-similarity is observed, providing evidence that the macroscopic wake behavior is strongly dependent on the local Mach number of the flow, in the drop frame of reference. Volume fraction contours of the simulations of Drop 3 and Drop 6B are directly compared. Differences in the wake flow are attributed to the strong influence of Mach number on both the flow expansion angle about the equator of the drop and the stability of the shear layers. This was further demonstrated with the removal of all liquid phenomena in the computations of supersonic flow about a hard sphere. Increasing the Mach number in the low-supersonic range ($M_{2LF} \approx 1-2$) results in both larger expansion angles and greater shear-layer wake stability, and thus a shorter wake.

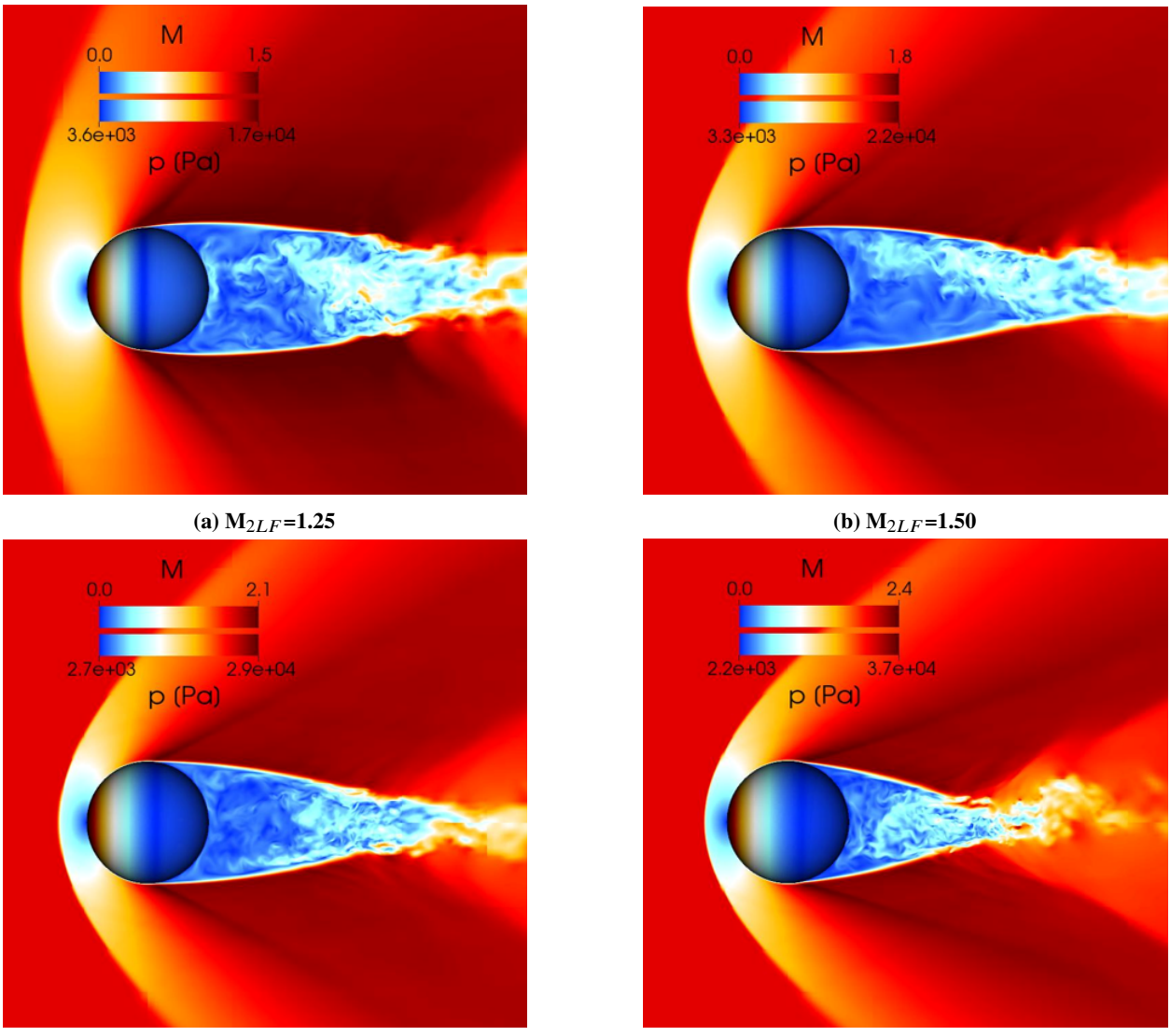

(a) M_{2LF}=1.25 **(b) M_{2LF}=1.50**

(c) M_{2LF}=1.75 **(d) M_{2LF}=2.00**

Fig. 5 Cut planes showing Mach number contours and surface pressure contours at different Mach numbers.

Acknowledgments

J. D. Langhorn, A. R. Dworzanczyk, A. J. Marino, and N. J. Parziale were supported by ONR-MURI Grant N00014-20-1-2682. M. Viqueira-Moreira and C. Brehm gratefully acknowledge funding for this work from the Office of Naval Research grant no. N00014-22-1-2443 & N00014-25-1-2355. Dr. Eric Marineau of Code 351 is the Program Officer for all grants.

References

[1] Dworzanczyk, A. R., Viqueira-Moreira, M., Langhorn, J. D., Libeau, M. A., Brehm, C., and Parziale, N. J., "On aerobreakup in the stagnation region of high-Mach-number flow over a bluff body," *Journal of Fluid Mechanics*, Vol. 1002, 2025, p. A1. https://doi.org/10.1017/jfm.2024.1092.

[2] Hanthanan Arachchilage, K. M., "Multiphase Flow Modeling of Molten Metal Atomization at High Gas Pressure," Ph.D. thesis, University of Central Florida, 2019.

[3] Lagutkin, S., Achelis, L., Sheikhaliev, S., Uhlenwinkel, V., and Srivastava, V., "Atomization process for metal powder," *Materials Science and Engineering: A*, Vol. 383, No. 1, 2004, pp. 1–6. https://doi.org/10.1016/j.msea.2004.02.059.

[4] Mates, S. P., and Settles, G. S., "A Study of Liquid Metal Atomization Using Close-Coupled Nozzles, Part 2: Atomization Behavior," *Atomization and Sprays*, Vol. 15, No. 1, 2005, pp. 41–60. https://doi.org/10.1615/AtomizSpr.v15.i1.30.

[5] Middlebrooks, J., Avgoustopoulos, C., Black, W., Allen, R. C., and McFarland, J. A., "Droplet and multiphase effects in a shock-driven hydrodynamic instability with reshock," *Experiments in Fluids*, Vol. 59, No. 98, 2018. https://doi.org/10.1007/s00348-018-2547-7.

[6] Salauddin, S., Morales, A. J., Hytovick, R., Burke, R., Malik, V., Patten, J., Schroeder, S., and Ahmed, K. A., "Detonation and shock-induced breakup characteristics of RP-2 liquid droplets," *Shock Waves*, Vol. 33, No. 3, 2023, pp. 191–203. https://doi.org/10.1007/s00193-023-01132-7.

[7] Young, C. J., Duke-Walker, V. O., and McFarland, J. A., "Droplet breakup and evaporation in liquid-fueled detonations," *Experimental Thermal and Fluid Science*, Vol. 160, 2025, p. 111324. https://doi.org/https://doi.org/10.1016/j.expthermflusci.2024.111324.

[8] Moylan, B., Landrum, B., and Russell, G., "Investigation of the Physical Phenomena Associated with Rain Impacts on Supersonic and Hypersonic Flight Vehicles," *Procedia Engineering*, Vol. 58, 2013, pp. 223–231. https://doi.org/10.1016/j.proeng.2013.05.026.

[9] Dworzanczyk, A., Parziale, N. J., Mueschke, N. J., Grosch, D. J., and Bueno, P., "Material Survivability on Launch of Slender Ballistic Range Projectiles," *Proceedings of AIAA Scitech 2022*, AIAA-2022-0772, San Diego, California and Virtual Event, 2022. https://doi.org/10.2514/6.2022-0772.

[10] Viqueira-Moreira, M., Dworzanczyk, A., Parziale, N. J., and Brehm, C., "Numerical investigation of droplet aerobreakup and impingement experiments at Mach 5," *AIAA AVIATION 2023 Forum*, 2023, p. 4251.

[11] Viqueira-Moreira, M., Gonuleri, R. K., Leigh, J. R., Watson, K., Guven, I., and Brehm, C., "Higher-Order Simulations of Droplet-Shock Interaction, Aerobreakup and Impingement at High Mach Numbers," *AIAA SCITECH 2023 Forum*, 2023, p. 2305. https://doi.org/10.2514/6.2023-2305.

[12] Dworzanczyk, A., Parziale, N. J., Croft, C. J., Wise, D. R., and Libeau, M. A., "High-Speed Imaging of Interaction of Liquid Drops with Hypersonic Projectiles," *Proceedings of AIAA Aviation 2023*, AIAA-2023-4248, San Diego, California and Virtual Event, 2023. https://doi.org/10.2514/6.2023-4248.

[13] Dworzanczyk, A., Parziale, N. J., Mueschke, N. J., Grosch, D. J., and Bueno, P., "High-Speed Imaging of Droplet Impact on a Hypervelocity Projectile," *Proceedings of AIAA Scitech 2023*, AIAA-2023-0464, National Harbor, Maryland and Virtual Event, 2023. https://doi.org/10.2514/6.2023-0464.

[14] Dworzanczyk, A. R., Langhorn, J. D., Parziale, N. J., Libeau, M. A., Brehm, C., and Viqueira-Moreira, M., "Instability Analysis of Drop Aerobreakup at High Mach Number," *Proceedings of AIAA SciTech 2025*, AIAA-2025-1504, Orlando, Florida, 2025. https://doi.org/10.2514/6.2025-1504.

[15] Pilch, M., and Erdman, C. A., "Use of breakup time data and velocity history data to predict the maximum size of stable fragments for acceleration-induced breakup of a liquid drop," *International Journal of Multiphase Flow*, Vol. 13, No. 6, 1987, pp. 741–757. https://doi.org/10.1016/0301-9322(87)90063-2.

[16] Tadjdeh, Y., "Navy's Electromagnetic Railgun Project Progressing," *National Defense*, Vol. 102, No. 764, 2017, pp. 33–34.

[17] Viqueira-Moreira, M., Stoffel, T. D., Poovathingal, S. J., and Brehm, C., "Validation of a High-Order Diffuse Interface Multi-Phase Method for High-Speed Droplet Shock Interaction and Impingement," *AIAA AVIATION 2022 Forum*, 2022, p. 3922. https://doi.org/10.2514/6.2022-3922.

[18] Stoffel, T. D., Viqueira-Moreira, M., Brehm, C., and Poovathingal, S. J., "Application of a Diffuse Interface Multiphase Method for High Temperature and Hypersonic Flows with Phase Change," *AIAA SCITECH 2023 Forum*, 2023, p. 2305. https://doi.org/10.2514/6.2023-4250.

[19] Allaire, G., Clerc, S., and Kokh, S., "A five-equation model for the simulation of interfaces between compressible fluids," *Journal of Computational Physics*, Vol. 181, No. 2, 2002, pp. 577–616. https://doi.org/10.1006/jcph.2002.7143.

[20] Wong, M. L., Angel, J. B., Barad, M. F., and Kiris, C. C., "A positivity-preserving high-order weighted compact nonlinear scheme for compressible gas-liquid flows," *Journal of Computational Physics*, Vol. 444, 2021, p. 110569. https://doi.org/10.1016/j.jcp.2021.110569.

[21] Brehm, C., and Fasel, H. F., "A Novel Concept for the Design of Immersed Interface Methods," *Journal of Computational Physics*, Vol. 242, 2013, pp. 234–267.

[22] Brehm, C., Hader, C., and Fasel, H. F., "A Locally Stablilized Immersed Boundary Method for the Compressible Navier-Stokes Equations," *Journal of Computational Physics*, Vol. 295, 2015, pp. 475–504. https://doi.org/10.1016/j.jcp.2015.04.023.

[23] Brehm, C., Barad, M. F., and Kiris, C. C., "Development of Immersed Boundary Computational Aeroacoustic Predication Capabilities for Open-Rotor Noise," *Journal of Computational Physics*, Vol. 388, 2019, pp. 690–716. https://doi.org/10.1016/j.jcp.2019.02.011.

[24] Michalke, A., "The instability of free shear layers," *Progress in Aerospace Sciences*, Vol. 12, 1972, p. 213–216. https://doi.org/10.1016/0376-0421(72)90005-x, URL http://dx.doi.org/10.1016/0376-0421(72)90005-X.

[25] Chen, J. H., Cantwell, B. J., and Mansour, N. N., "The effect of Mach number on the stability of a plane supersonic wake," *Physics of Fluids A: Fluid Dynamics*, Vol. 2, No. 6, 1990. https://doi.org/10.1063/1.857606, URL http://dx.doi.org/10.1063/1.857606.

[26] Papamoschou, D. and Roshko, A., "The compressible turbulent shear layer: an experimental study," *Journal of Fluid Mechanics*, Vol. 197, 1988, pp. 453–477. https://doi.org/10.1017/S0022112088003325.

[27] Chapman, D. R., "An Analysis of Base Pressure at Supersonic Velocities and Comparison with Experiment," NACA TR-1051, 1951.

[28] Kurtz, D. W., and Kerr, W. R., "Base Pressure Distribution of Two Blunted Cones at Mach Numbers From 0.3 to 0.8 and 1.81 to 3.51," NASA CR-100427, 1968.

[29] Carpenter, P. W., and Tabakoff, W., "Survey and Evaluation of Supersonic Base Flow Theories," NASA CR-97129, 1968.

[30] van Noordt, W., McQuaid, J., Larsson, J., and Brehm, C., "GPU-Accelerated Simulations of Turbulent Flows With the Immersed Boundary Method," *AIAA AVIATION FORUM AND ASCEND 2024*, 2024, p. 3536. https://doi.org/10.2514/6.2024-3536.